Spectroscopic determination of phase and space resolved EEDFs in RF discharges

T. Gans[*], V. Schulz-von der Gathen, and H.F. Döbele

Universität Essen, Institut für Laser- und Plasmaphysik, Universitätsstr. 5, 45117 Essen, Germany

[*]*present address: Dublin City University, Plasma Research Laboratory, Glasnevin, Dublin 9, Ireland*
electronic address: timo.gans@web.de

Abstract: *We report on a novel spectroscopic diagnostic technique for phase and space resolved measurements of the electron energy distribution function (EEDF) of energetic (>12eV) electrons in RF discharges. These electrons are of particular interest since they dominate excitation and ionization processes. The technique is based on time dependent measurements during the RF cycle of excited state populations of rare gases admixed in small amounts as tracer gases. These measurements yield, in combination with an analytical model, detailed information on the excitation processes. The time dependent model takes into account: electron impact excitation, heavy particle collisional excitation, radiation-less collisional de-excitation (quenching), radiation trapping and cascade processes from higher electronic states. First results are presented for a hydrogen capacitively coupled RF discharge excited with a frequency of 13.56 MHz. The EEDF of electrons accelerated in the sheath region can be described by a shifted Maxwellian distribution function with a drift component in the direction of the electric field. In contrast to other electron specific diagnostic techniques, e.g. Thomson scattering or probe measurements, phase resolved optical emission spectroscopy (PROES) allows us, for the first time, to overcome the difficulties connected with the low densities (10^7-10^9 cm^{-3}) and the transient character of energetic electrons in the sheath region. In general the presented diagnostic technique can also be applied to other RF excited discharges.*

Introduction

RF discharges bear considerable application potential. They are frequently applied in surface modification (cleaning, conditioning), the generation of microstructures (etching) and in layer deposition [1]. The electron energy distribution function (EEDF) is not only a key parameter for understanding basic discharge mechanisms like electron heating, it also governs dissociation, excitation and ionization processes with relevance in plasma applications. Measurements of energetic electrons exceeding the appropriate threshold energies of these processes are fairly complicated due to their low densities and transient character. Phase resolved optical emission spectroscopy (PROES) clearly shows the transient character by investigations of excited states with lifetimes noticeable shorter than the RF period [2-4].

The EEDF is most commonly measured by Langmuir probes [5-8]. However, these can not provide the required time resolution on a ns scale for phase resolved measurements. Further problems can be the invasive character of probes, especially in reactive gases, also measurement problems due to perturbations by RF fields and the limited sensitivity for energetic electrons. Measurements of the EEDF by Thomson scattering can provide the required temporal resolution. However, they give no access to the low densities of transient energetic electrons, because of the weak Thomson scattering signal superposed on strong signals of scattering processes on neutral particles, especially in molecular process gases [9, 10].

In the last years, optical emission spectroscopy (OES) has been successfully applied for measurements of EEDFs under steady state conditions [11-14]. The general approach is to compare population densities of states that are excited by electrons from different parts of the EEDF. In this work, the approach is extended for phase and space resolved measurements of transient, energetic, directed electrons in RF discharges. This novel diagnostic became possible by the availability of improved data on electron impact excitation cross sections, cascading contributions from higher electronic states and coefficients for radiation-less collisional de-excitation (quenching) measured recently in electron beam [15-18] and other PROES experiments [19]. An analytical model for the

population dynamics within the RF cycle and an analytical approach for the EEDF are discussed below. The presented diagnostic technique is applied to a hydrogen capacitively coupled RF (CCRF) discharge, because of its pronounced excitation dynamics and broad application potential.

Experiment

The experimental setup is described in detail elsewhere [20]. The discharge chamber is similar to the GEC reference cell [21]. The flat cooled stainless steel electrodes, 100 mm in diameter, are 25 mm apart. The plasma is generated with an RF power supply (ENI ACG 6B) and a matching unit (ENI MW-10 D), at a frequency of 13.56 MHz, in an asymmetric configuration with one electrode grounded. The measurements are performed at an RF power of 100 W and a total gas pressure of 148 Pa. A small amount (5%) of a rare gas mixture (10% Kr, 20% Ar, 30% Ne, 40% He) is added as tracer gas to the hydrogen discharge. An unequal mixture is used, since the influence of rare gas admixtures on the investigated discharge was found to increase with decreasing ionization energy of the rare gas. For added mixtures smaller than 5% no influence was observable. The discharge axis is imaged onto the entrance slit of a 2m-spectrograph (Jenoptik PGS 2, 1302 mm^{-1} grating), see Fig. 1.

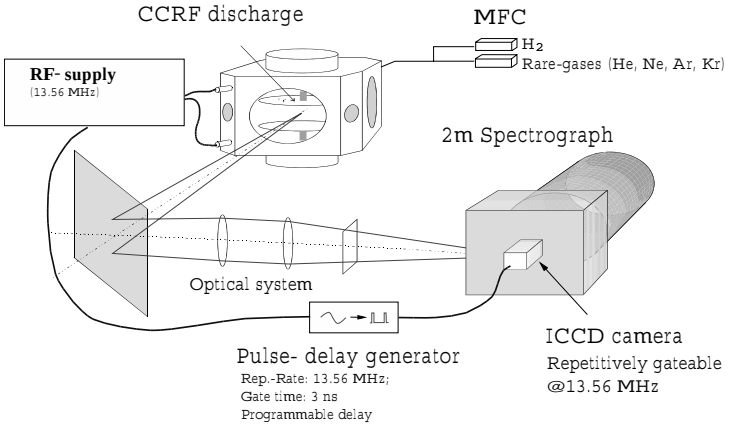

Figure 1*: Experimental setup of the discharge chamber and the electronic and optical components for PROES.*

A fast gateable ICCD-camera (Picostar, LaVision GmbH) samples spectral intervals of about 4.5 nm with a spectral resolution of 0.03 nm and a spatial resolution of about 0.5 mm. This spectral resolution allows us to separate the tracer gas emission lines from numerous molecular hydrogen emission lines. Phase-resolved measurements are possible by synchronization of the camera measurement gate to the RF frequency. The intensities measured in the gate time of 3 ns can be integrated over many RF cycles for a certain phase setting. Measurements of faint tracer gas emission lines are feasible due to the high repetition rate (13.56 MHz) of the ICCD-camera which enables us to use every RF cycle for integration. The entire optical system is absolutely calibrated with a tungsten ribbon lamp (Osram WI 17/G).

Excitation dynamics

In contrast to the standard corona model commonly used for OES of stationary low density plasmas, PROES requires a time dependent model based on rate equations to take into account the transient character of the exciting electrons. Electron impact $\left(E^e(t)\right)$ and heavy particle collisional excitation $\left(E^H(t)\right)$ out of the ground state are described by the excitation function $E(t) = E^e(t) + E^H(t)$. Excitation out of metastable or resonant states is negligible because of their low population density in molecular discharges in the investigated pressure range due to effective quenching processes [22]. For an excited state *i* not populated by cascade processes the excita-

tion function $E_i(t)$ can be determined directly from the measured number of photons per unit volume and unit time $\dot{n}_{Ph,i}(t)$:

$$E_i(t) = \frac{1}{n_0 A_{ik}} \left(\frac{d\dot{n}_{Ph,i}(t)}{dt} + A_i \dot{n}_{Ph,i}(t) \right). \qquad (1)$$

Here, $\dot{n}_{Ph,i}(t) = A_{ik} n_i(t)$ is given by the transition probability A_{ik} of the observed emission and the population density of the investigated state $n_i(t)$; n_0 is the ground state density. The effective decay rate A_i takes into account spontaneous emission, radiation trapping and quenching:

$$A_i = \sum_k A_{ik} g_{ik} + \sum_q k_q n_q \,, \qquad (2)$$

where g_{ik} is the so called escape factor [23, 24] and k_q the quenching coefficient with the species q of density n_q. Under the conditions in this work all transitions to the ground state are optical thick $(g_{ik} = 0)$ and all other transitions are optical thin $(g_{ik} = 1)$.

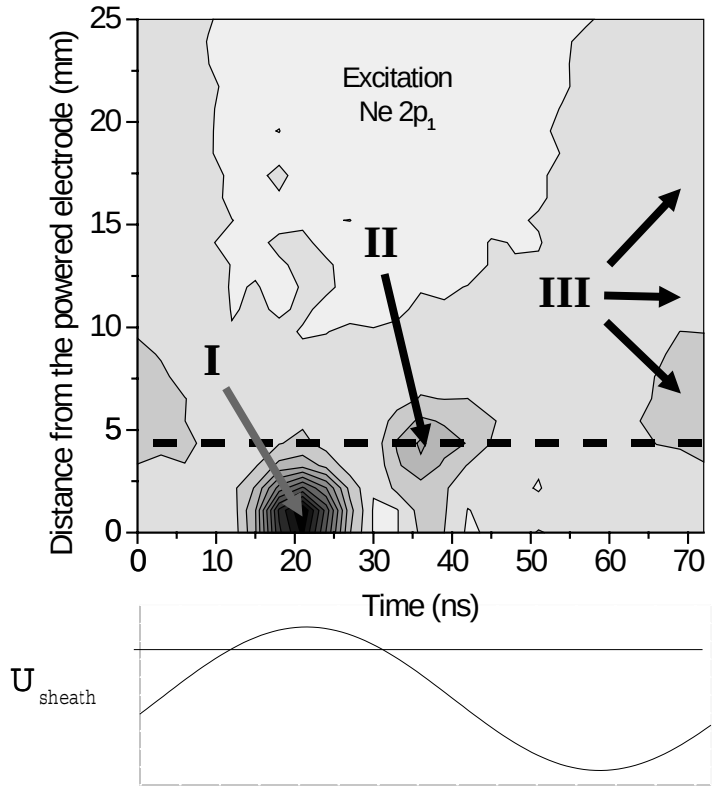

Figure 2: *Phase and space resolved excitation of the Ne $2p_1$ state in a hydrogen CCRF discharge at 141 Pa and 100 W. Also shown is a sketch of the sheath voltage as measured by Czarnetzki et al. [25, 26]*

Fig. 2 displays the phase and space resolved excitation of the Neon $2p_1$ state which is practically free of population by cascades [18]. The abscissa comprises one RF cycle and the transverse axis indicates the distance from the powered electrode. Different electron impact excitation processes (I-III) can be explained on the basis of E-field measurements [25, 26]. Process I is caused by

a field reversal across the space charge sheath, typical for hydrogen RF discharges. During this phase electrons are accelerated towards the powered electrode and induce a strong impact excitation. The excitation by process II is due to sheath expansion heating of electrons moving to the plasma bulk, when the sheath potential becomes negative again. Excitation process III results from secondary electrons created by ion impact. Due to the small mass of hydrogen ions they are able to follow the applied electric field [27]. Thus, time dependent ion bombardment determines the creation of secondary electrons at the electrode surface. During the phase of maximum bombardment the high sheath potential of several hundred Volts results in an acceleration of electrons and electron multiplication by ionization. The high energetic directed electrons created in the sheath region also induce excitation when they enter the plasma bulk (process III).

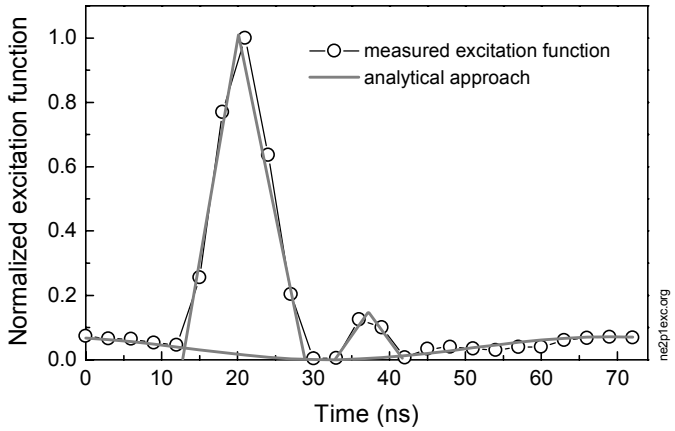

Figure 3*: Excitation function of the Neon 2p$_1$ state close to the powered electrode including analytical approximations for excitation during the field reversal phase, the sheath expansion phase and by heavy particle collisions.*

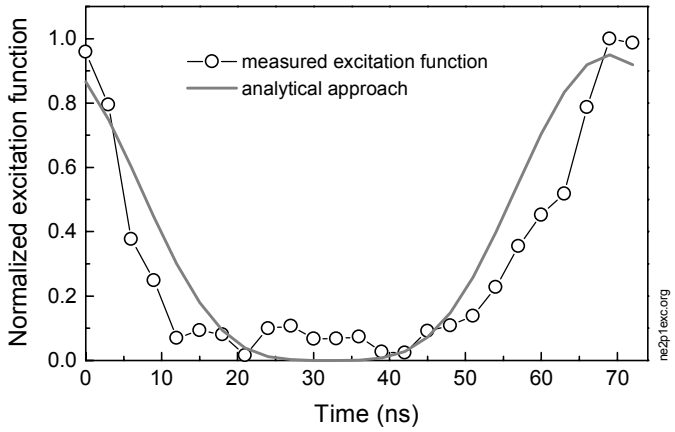

Figure 4*: Excitation function of the Neon 2p$_1$ state within the plasma bulk including an analytical approximation for excitation by high energetic secondary electrons.*

Fig. 3 and fig. 4 show sections of fig. 2 close to the powered electrode and within the plasma bulk, respectively. The time dependence of excitation during the field reversal phase and the sheath expansion phase can be approximated by triangular functions as indicated in fig. 3. The excitation by secondary electrons in fig. 4 follows a squared sinusoidal function since ion bombardment and

acceleration in the sheath are both governed by sinusoidal functions. The weak sinusoidal excitation in fig. 3 is due to heavy particle collisions of energetic (>100 eV) hydrogen atoms with the background gas [19, 27].

Population dynamics of excited states

For quantitative investigations of the EEDF cascade processes can be substantial [19], particularly in the investigated pressure range (partial rare gas pressure: 0.75 - 3 Pa) [15-19]. The population density $n_i(t)$ of the investigated state *i* can be described by the following rate equation including cascades from state *c*:

$$\frac{dn_i(t)}{dt} = n_0 E_i(t) - A_i n_i(t) + A_{ci} n_c(t) \,. \qquad (3)$$

The population density $n_c(t)$ obeys a rate equation analogous to eq. 3, without cascade processes:

$$\frac{dn_c(t)}{dt} = n_0 E_c(t) - A_c n_c(t) \,. \qquad (4)$$

The coupled differential equations for the investigated state *i* and the cascade state *c* can be solved in a general manner for the periodic boundary conditions of the RF discharge $\left(n_{i,c}(t) = n_{i,c}(t + T_{RF})\right)$:

$$\begin{aligned} n_i(t) &= n_0 \left(\frac{\widetilde{E}_i(T_{RF}, A_i) e^{-A_i T_{RF}}}{1 - e^{-A_i T_{RF}}} + \widetilde{E}_i(t, A_i) \right) e^{-A_i t} \\ &+ \frac{n_0 A_{ci}}{A_i - A_c} \left[\left(\frac{\widetilde{E}_c(T_{RF}, A_c) e^{-A_c T_{RF}}}{1 - e^{-A_c T_{RF}}} + \widetilde{E}_c(t, A_c) \right) e^{-A_c t} - \left(\frac{\widetilde{E}_c(T_{RF}, A_i) e^{-A_i T_{RF}}}{1 - e^{-A_i T_{RF}}} + \widetilde{E}_c(t, A_i) \right) e^{-A_i t} \right] \end{aligned} \qquad (5)$$

Here, the abbreviation $\widetilde{E}_x(t, A_y) = \int_0^t E_x(t') e^{A_y t'} dt'$ has been used. Together with the above given analytical approximations for the time dependencies of the various excitation processes, eq. 5 allows us to determine the amplitudes of excitation processes even for states fed by cascade processes. Additionally, this access to excitation functions is less sensitive to noise in measurements than the direct one (eq. 1), because derivatives of measured data are avoided.

Measurement of EEDFs

Excitation functions are measured for the following states:

State	λ [28]	E_{th} [28]	τ_i [28]	$A_{ik}\tau_i$ [28]	k_{H2} [19]
	(nm)	(eV)	(ns)		(10^{-10}cm^{3}s^{-1})
Kr $2p_5$	758.7	11.7	21.5	1	1.7
Kr $2p_2$	826.3	12.2	34.1	0.95	9.7
Ar $2p_1$	750.4	13.5	22.4	1	0.3
Ne $2p_6$	614.3	18.6	21.9	0.62	7.4
Ne $2p_1$	585.2	19.0	14.5	0.99	2.3
He 3^3S	706.5	22.7	36.1	1	9.6
He 3^1S	728.1	22.9	55.2	1	10.7

These states have excitation thresholds in the range from 11.7 eV to 22.9 eV, and their electron impact excitation cross sections as well as the contributions of cascades are accurately known [15-18]. The comparatively small cascade contribution to the population of these states justifies the neglect of second order cascade processes. Coefficients for quenching with molecular hydrogen and transition rates are taken from ref. [19] and ref. [28], respectively.
Comparison of measured excitation functions of these states yields information on the EEDF in an energy range even beyond the respective excitation thresholds because of the different shapes of the electron impact excitation cross sections, in particular for the singlet and triplet states of He. The gained information does not provide direct access to the EEDF, however, since the excitation function $E_i^{\,e}$ of the state *i* is given by the following integral over the energy dependent electron impact excitation cross section $\sigma_i(E)$ and the EEDF *f(E)*:

$$E_i^{\,e} = n_e \int_0^\infty \sigma_i(E) \sqrt{\frac{2E}{m_e}} f(E) dE \,. \qquad (6)$$

Here, n_e and m_e are the electron density and mass, respectively. This problem can be overcome by an analytical approach with a set of free parameters describing the shape of the EEDF. This set is varied until the calculated excitation function, from the EEDF and eq. 6, best fits to the measured excitation functions of all investigated states. The EEDF is commonly described by a Maxwellian or a Druyvesteynian distribution function with the electron temperature T_e as the only parameter. In ref. [11] a more general approach is proposed by introducing another free parameter *b*. This approach includes both a Maxwellian distribution (b=1) and a Druyvesteynian distribution (b=2):

$$f_b(E) = C_b \sqrt{E} \exp\left[- A_b \left(\frac{E}{k_B T_e} \right)^b \right]. \qquad (7)$$

Here, k_B is the Boltzmann constant and the effective electron temperature T_e is defined by the average electron energy $\langle E \rangle = \frac{3}{2} k_B T_e$. This definition and normalization determine A_b and C_b with the gamma function Γ as follows:

$$A_b = \left(\frac{2\Gamma\left(\frac{5}{2b}\right)}{3\Gamma\left(\frac{3}{2b}\right)} \right)^b, \qquad C_b = \frac{b A_b^{\frac{3}{2b}}}{(k_B T_e)^{1.5} \Gamma\left(\frac{3}{2b}\right)}. \qquad (8)$$

However, an appropriate description of electrons in the discharge considered has to take into account a drift velocity v_D in the direction of the electric field in the sheath region. Distribution functions including this drift component were found to reproduce the measured excitation functions much better than isotropic distribution functions. An anisotopic shifted Maxwellian distribution function $f_D(\vec{v})$, with two different 'temperatures' in the direction of the electric field (T_z) and perpendicular (T_r), is given by:

$$f_D(\vec{v}) = \frac{1}{\sqrt{\pi}^3 \theta_r^{\,2} \theta_z} \exp\left[- \left(\frac{v_x^{\,2} + v_y^{\,2}}{\theta_r^{\,2}} + \frac{(v_z - v_D)^2}{\theta_z^{\,2}} \right) \right]. \qquad (9)$$

Here, the following expression is used:

$$\theta_{r,z} = \sqrt{\frac{2k_B T_{r,z}}{m_e}} . \qquad (10)$$

Tests with this type of distribution function have shown that best agreement with measurements is obtained if the two temperatures are almost identical. The further analysis is, therefore, based on a shifted Maxwellian distribution function $f_D(E)$ with a single electron temperature T_e. Transformation from velocity space to energy space results in the following function with a drift energy E_D in the direction of the electric field:

$$f_D(E) = \frac{1}{2\sqrt{\pi\, k_B T_e E_D}} e^{-\frac{\left(\sqrt{E}-\sqrt{E_D}\right)^2}{k_B T_e}} \left(1 - e^{-\frac{4\sqrt{E \cdot E_D}}{k_B T_e}} \right). \qquad (11)$$

Note that for small drift energies this function converges to a regular isotropic Maxwellian distribution function.
Fig. 5 shows an example of obtaining the parameter set which describes the EEDF at maximum excitation during the field reversal phase. The deviation (defined as the standard deviation in percent) of the measured excitation functions and the calculated excitation functions under variation of the free parameters exhibits a clear minimum indicating a strong drift component. Furthermore, the figure shows that the drift energy component could be compensated partly, but not perfectly, by a higher electron temperature. This is obvious when the drift energy is set equal to zero. In this case the minimum deviation (on the abscissa) occurs at an electron temperature around 10 eV. The larger deviation of the pure Maxwellian distribution function is a systematic problem of all isotropic distribution functions mentioned above. All these functions decrease, in contrast to functions including a drift component, monotonically in a plot like fig. 6. The excitation of states with low threshold energies can, therefore, be overestimated, since a decrease to lower energies cannot be described by these functions.

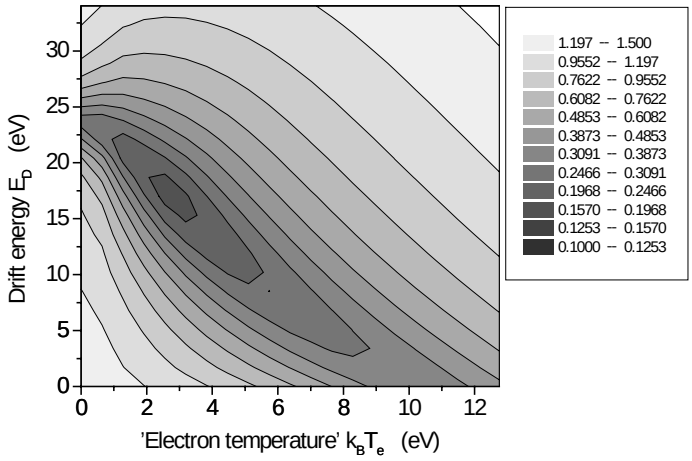

Figure 5: *Deviation of measured and calculated excitation functions under variation of the free parameters during the field reversal phase. The EEDF is obtained from the parameter set at minimum deviation.*

Results

Fig. 6 shows typical examples of EEDFs during the field reversal phase, the sheath expansion phase and of secondary electrons. The strong influence of the drift component can be clearly seen; note that a pure Maxwellian distribution function would be a straight line in this plot.

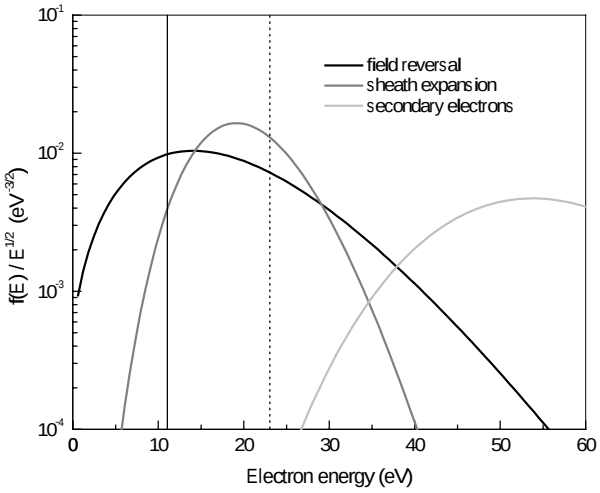

Figure 6: *Typical examples of EEDFs during the field reversal phase, the sheath expansion phase and EEDF of secondary electrons. The lowest and highest excitation thresholds of the investigated states are indicated by vertical lines.*

The obtained parameter sets describing the phase and space resolved EEDF are shown in fig. 7 for the various excitation processes at different phases of the RF-cycle. In the case of the secondary electrons the analysis tends to be unstable because of noisy data. However, only a weak dependence (<15%) of the drift energy is observable. The drift energy is, therefore, fixed to the value obtained close to the sheath boundary $(E_D = 55eV)$ to provide a stable analysis. The electron temperature of the secondary electrons increases from the sheath boundary to the grounded electrode.

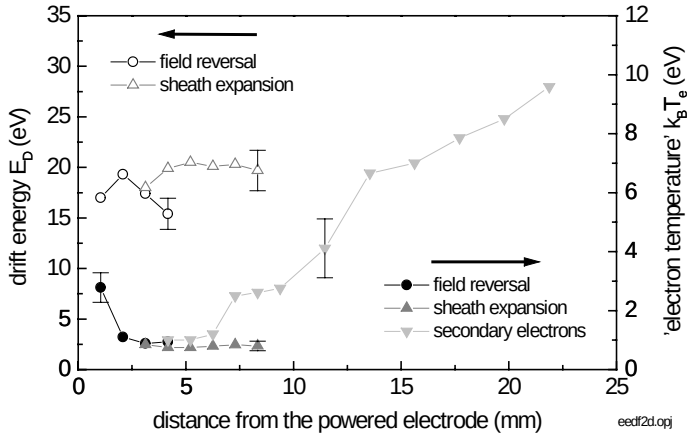

Figure 7*: Parameter sets describing the phase and space resolved EEDF for the various excitation processes. For the secondary electrons the drift energy is fixed to 55 eV, see text for details.*

This more isotropic character close to the grounded electrode can be explained by collisions in the plasma bulk. It is remarkable that the EEDF is nearly independent of the distance from the powered electrode during the sheath expansion phase. Furthermore, a very interesting phenomenon is ob-

servable close to the powered electrode during the field reversal phase. The drift energy drops slightly while the electron temperature increases strongly, which results in a more isotropic EEDF. The absolutely calibrated optical system yields, in addition to the shape of the EEDF, the electron density from the absolute value of the excitation. It is assumed that the EEDF can be described by the analytical approach and the obtained parameter set over the entire energy range which is not necessarily true for energies lower than the lowest excitation threshold as indicated in fig. 6. Phase and space resolved densities of electrons involved in the various excitation processes are shown in fig. 8.

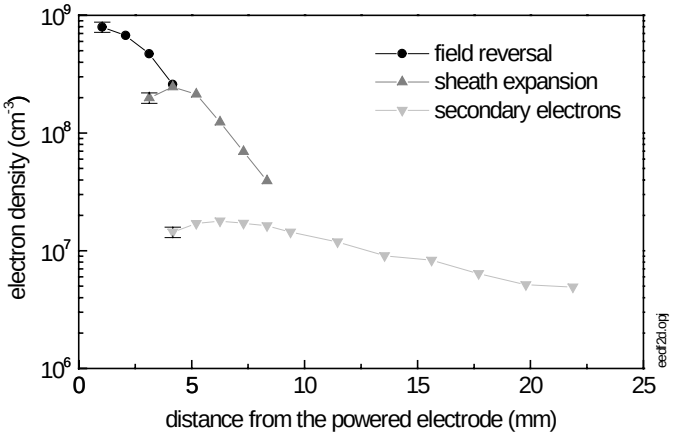

Figure 8*: Phase and space resolved densities of electrons involved in the various excitation processes.*

The electrons are accelerated by the electric field within the sheath region either towards the powered (field reversal) or the grounded electrode (sheath expansion and secondary electrons). These energetic electrons result in ionization within the sheath region as can be seen from increasing densities in the direction of the electron drift, see fig. 8. The densities of exciting electrons, during the sheath expansion phase and the secondary electrons, decrease within the plasma bulk due to collisions and no further energy gain. The time independent properties of isotropic bulk electrons are measured, with a commercial Langmuir probe system (Smart Probe, Scientific Systems), to be Maxwellian with a temperature of $(1.2 \pm 0.1) eV$ and a density of $(1.3 \pm 0.1) \cdot 10^{10} cm^{-3}$, respectively. These electrons contribute less than 5% to excitation and ionization processes because of their low temperature, although their density is higher by orders of magnitudes compared to that of the directed energetic electrons measured by PROES. Excitation and ionization processes are, therefore, completely dominated by time dependent directed electrons of high energy even in the plasma bulk itself.

Conclusion

We have demonstrated a novel spectroscopic method for phase and space resolved measurements of the EEDF in RF discharges. It is planned to apply this diagnostic technique beyond the present application to discharges in other gases, different pressure regimes and other types of RF discharges like inductively coupled plasmas or dual frequency capacitively coupled plasmas with an analytical approach for the EEDF adapted to the respective geometry.

Acknowledgment

The authors thank Chun C. Lin (University of Wisconsin, Madison) for helpful discussions and C. Fischer and J. Leistikow for skillful technical assistance. Support by the 'Deutsche Forschungsgemeinschaft' in the frame of SFB 191 is gratefully acknowledged.

References

[1] M.A. Lieberman and A.J. Lichtenberg, Principles of Plasma Discharges and Materials Processing, John Wiley & Sons Inc., New York (1994)
[2] T. Gans, Chun C. Lin, V. Schulz-von der Gathen, and H.F. Döbele, J. Phys. D: Appl. Phys. 34 (2001) L1
[3] C.M.O. Mahony and W.G. Graham, IEEE Trans. Plasma Sci. 27 (1999) 72
[4] V.A. Kadetov, U. Czarnetzki, H.F. Döbele, Proceedings ESCAMPIG 16 Vol. 1, Grenoble, France (2002) p. 251
[5] I. Langmuir, Gen. Electr. Rev. 26 (1923) 731
[6] M.J. Druyvesteyn, Z. Phys. 64 (1930) 790
[7] N. Hershkowitz, Plasma Diagnostics - Discharge Parameters and Chemistry, Bd. 1, Kap. 3, S. 12, Academic Press, San Diego (1989)
[8] V.A. Godyak, Plasma - Surface Interaction and Processing of Materials, NATO Advanced Institutes Series E 176 (1990) 95
[9] H. Kunze, Plasma Diagnostics, In Lochte-Holtgreven, North-Holland, Amsterdam (1968)
[10] M.D. Bowden et al., J. Appl. Phys. 73 (1993) 2732
[11] K. Behringer and U. Fantz, J. Phys. D: Appl. Phys. 27 (1994) 2128
[12] M.V. Malyshev and V.M. Donnelly, J. Vac. Sci. Technol. A 15 (1997) 550
[13] M.V. Malyshev and V.M. Donnelly, Phys. Rev. E 60 (1999) 6016
[14] I.P. Vinogradov, Plasma Sources Sci. Technol. 8 (1999) 299
[15] I.P. Bogdanova and S.V. Yurgenson, Opt. Spektrosk. 61 (1986) 241
[16] J.E. Chilton, J.B. Boffard, R.S. Schappe, and C.C. Lin, Phys. Rev. A 57 (1998) 267
[17] J.E. Chilton, M.D. Stewart, Jr., and C.C. Lin, Phys. Rev. A 62 (2000) 32714
[18] J.E. Chilton, M.D. Stewart, Jr., and C.C. Lin, Phys. Rev. A 61 (2000) 52708
[19] T. Gans, Chun C. Lin, V. Schulz-von der Gathen, and H.F. Döbele, Phys. Rev. A 67 (2003) 12707
[20] T. Gans, V. Schulz-von der Gathen, and H.F. Döbele, Plasma Sources Sci. Technol. 10 (2001) 17
[21] P.J. Hargis et al., Rev. Sci. Instrum. 65 (1994) 140
[22] H.M. Katsch, E. Quandt and Th. Schneider, Plasma Phys. Control. Fusion 38 (1996) 183
[23] R.H. Huddlestone and S.L. Leonard, Plasma Diagnostic Techniques, Academic Press (1965)
[24] A. Anders, A Formulary for Plasma Physics, Akademie-Verlag, Berlin (1990)
[25] U. Czarnetzki, D. Luggenhölscher, and H.F. Döbele, Plasma Sources Sci. Technol. 8 (1999) 230
[26] U. Czarnetzki, D. Luggenhölscher, and H.F. Döbele, Appl. Phys. A 72 (2001) 509
[27] T. Gans, V. Schulz-von der Gathen, U. Czarnetzki, and H.F. Döbele, Contrib. Plasma Phys. 42 (2002) 596
[28] NIST atomic spectra database http://physics.nist.gov/cgi-bin/AtData/main_asd